SINTEF
PROCEEDINGS
2

Proceedings of the 12th International Conference on Computational Fluid Dynamics in the Oil & Gas, Metallurgical and Process Industries

Progress in Applied CFD – CFD2017

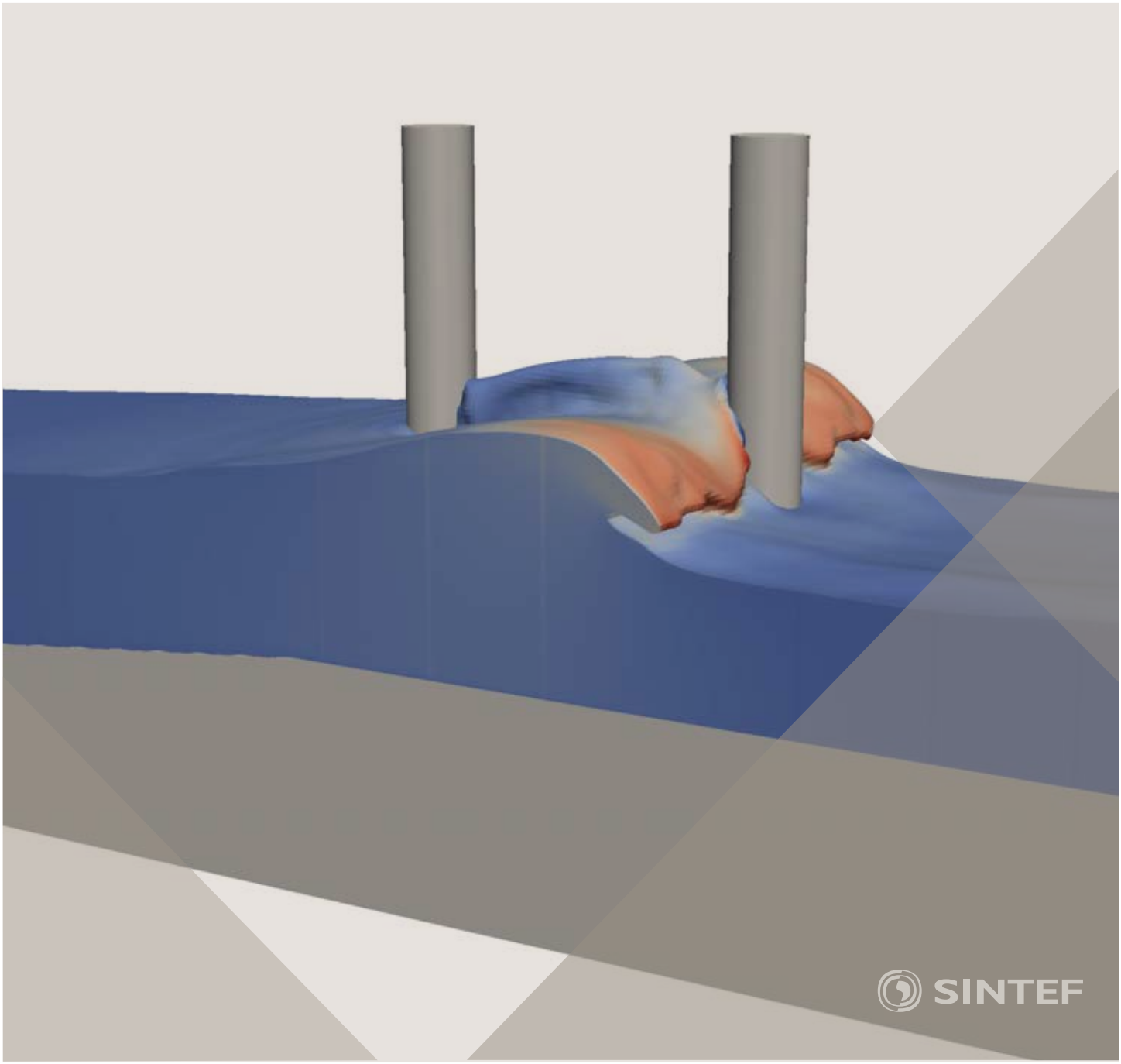

SINTEF Proceedings

Editors:
Jan Erik Olsen and Stein Tore Johansen

Progress in Applied CFD – CFD2017

Proceedings of the 12th International Conference on Computational Fluid Dynamics in the Oil & Gas, Metallurgical and Process Industries

SINTEF Academic Press

SINTEF Proceedings no 2
Editors: Jan Erik Olsen and Stein Tore Johansen
Progress in Applied CFD – CFD2017
Selected papers from 10th International Conference on Computational Fluid Dynamics in the Oil & Gas, Metallurgical and Process Industries

Key words:
CFD, Flow, Modelling

Cover, illustration: Arun Kamath

ISSN 2387-4295 (online)
ISBN 978-82-536-1544-8 (pdf)

SINTEF Academic Press
Address: Forskningsveien 3 B
PO Box 124 Blindern
N-0314 OSLO
Tel: +47 73 59 30 00
Fax: +47 22 96 55 08

www.sintef.no/byggforsk
www.sintefbok.no

SINTEF Proceedings
SINTEF Proceedings is a serial publication for peer-reviewed conference proceedings on a variety of scientific topics.
The processes of peer-reviewing of papers published in SINTEF Proceedings are administered by the conference organizers and proceedings editors. Detailed procedures will vary according to custom and practice in each scientific community.

PREFACE

This book contains all manuscripts approved by the reviewers and the organizing committee of the 12th International Conference on Computational Fluid Dynamics in the Oil & Gas, Metallurgical and Process Industries. The conference was hosted by SINTEF in Trondheim in May/June 2017 and is also known as CFD2017 for short. The conference series was initiated by CSIRO and Phil Schwarz in 1997. So far the conference has been alternating between CSIRO in Melbourne and SINTEF in Trondheim. The conferences focuses on the application of CFD in the oil and gas industries, metal production, mineral processing, power generation, chemicals and other process industries. In addition pragmatic modelling concepts and bio-mechanical applications have become an important part of the conference. The papers in this book demonstrate the current progress in applied CFD.

The conference papers undergo a review process involving two experts. Only papers accepted by the reviewers are included in the proceedings. 108 contributions were presented at the conference together with six keynote presentations. A majority of these contributions are presented by their manuscript in this collection (a few were granted to present without an accompanying manuscript).

The organizing committee would like to thank everyone who has helped with review of manuscripts, all those who helped to promote the conference and all authors who have submitted scientific contributions. We are also grateful for the support from the conference sponsors: ANSYS, SFI Metal Production and NanoSim.

Stein Tore Johansen & Jan Erik Olsen

Organizing committee:

Conference chairman: Prof. Stein Tore Johansen
Conference coordinator: Dr. Jan Erik Olsen
Dr. Bernhard Müller
Dr.Sigrid Karstad Dahl
Dr.Shahriar Amini
Dr.Ernst Meese
Dr.Josip Zoric
Dr.Jannike Solsvik
Dr.Peter Witt

Scientific committee:

Stein Tore Johansen, SINTEF/NTNU
Bernhard Müller, NTNU
Phil Schwarz, CSIRO
Akio Tomiyama, Kobe University
Hans Kuipers, Eindhoven University of Technology
Jinghai Li, Chinese Academy of Science
Markus Braun, Ansys
Simon Lo, CD-adapco
Patrick Segers, Universiteit Gent
Jiyuan Tu, RMIT
Jos Derksen, University of Aberdeen
Dmitry Eskin, Schlumberger-Doll Research
Pär Jönsson, KTH
Stefan Pirker, Johannes Kepler University
Josip Zoric, SINTEF

CONTENTS

SIMULATION OF DISPERSION OF IMMISCIBLE FLUIDS IN A TURBULENT COUETTE FLOW

Alexander VIKHANSKY[1] , Dmitry ESKIN[2]*

[1]Siemens PLM Software, Didcot, UK

[2] Schlumberger-Doll Research, Cambridge, MA, USA

* E-mail: deskin@slb.com

ABSTRACT

Dispersion of immiscible fluids in a Couette device, in which the inner cylinder rotates whereas the outer one is immobile, is modelled. Two different modelling approaches are employed. The 1st approach is based on solving a one-dimensional Advection-Diffusion-Population Balance equation. An influence of upper and bottom Couette device covers (the so-called end effect) is ignored in this case. The Prandtl mixing length model of turbulence, employed for modelling of a Couette flow field, allows obtaining an analytical expression for calculation of the energy dissipation rate distribution across Couette device gap. Fixed Pivot method is employed for numerical solution of the population balance equation.

The 2nd approach is based on the CFD-population balance A-MuSiG method, recently implemented into the STAR-CCM+ code of Siemens PLM Software. The Reynolds stress turbulence model along with the Daly & Harlow transport model are employed for modelling two-dimensional axisymmetric flow field in a Couette device.

In the present work, modelling is limited to only droplet breakup; i.e., only non-coalescing droplets are considered. A modified droplet breakup model of Coulaloglou and Tavlarides (1977) is employed for all the computations.

Computed droplet size distributions are compared with those obtained in a laboratory Couette device of a relatively small height that is a cause of the significant end effect. Dispersion of water droplets in silicone oil is studied. Coalescence is suppressed by a surfactant. The experimental droplet size distributions are reasonably well fitted by both the models employed.

The most significant advantage of the 3-D computations over the 1-D modelling is accounting for the end effect, that in its turn affects both velocity and energy dissipation rate distributions over the Couette device gap. Also, to better fit the experimental data, a weak coalescence was formally introduced into the 3-D computational code.

Keywords: Breakup, Dispersion, Droplets, Modelling, Population Balance, Turbulence

NOMENCLATURE

Greek Symbols

α Dispersed phase volume fraction

β Droplet breakup density function

δ_{in} Thickness of the viscous layer at the inner Couette device wall, [m]

δ_o Thicknesses of the viscous layers at the outer Couettte device wall, [m]

ε Energy dissipation rate per unit mass, [W/kg]

ρ Density, [kg/m^3].

μ Dynamic viscosity, [kg/m s]

τ_R Reynolds stress, [Pa]

τ_{win} Shear stress at the outer cylinder wall, [Pa]

Ω Inner cylinder rotation speed, [Hz]

υ Droplet volume, [m^3]

Latin Symbols

D Turbulent diffusivity of a droplet, [m^2/s]

d Droplet diameter, [Pa]

f_{bv} Breakup volume fraction

G Droplet breakup rate, [1/s]

H Width of the Couette device gap, [m]

L Couette device height, [m]

M Maximum number of size fractions

$\dot{m}$ Mass transfer rate between size fractions, [kg/m^3/s]

N Number concentration of droplets per unit volume, [1/m^3]

P Pressure, [Pa]

q Number flux of droplets, [1/m^2/s]

R Radius of the outer cylinder of a Couette device, [m]

R_m Radius of the gap centreline, [m]

r_{in} Radius of the inner cylinder of a Couette device, [m]

Re Couette device Reynolds number

u Velocity of a droplet averaged over a size fraction, [m/s]

u_{o*} Friction velocity at the outer cylinder wall, [m/s]

v Radial velocity component of a droplet, [m/s]

We Weber number

w Droplet fluctuation velocity, [m/s]

Sub/superscripts.

cr	critical
d	droplet
f	fluid
i, j	size fraction number

INTRODUCTION

Emulsification (emulsion formation) is a process of dispersion of one immiscible fluid in another one, and also an important stage of many technologies. In some cases, emulsions are produced intentionally when high viscosity fluids are required for some purposes. For example, emulsions are widely used as different components in food industry, or in petroleum industry as displacing fluids for enhanced oil recovery as well as fracturing fluids for hydraulic fracturing. However, frequently, emulsion formation is a highly undesired phenomenon. An example is emulsion formation during oil production. Water almost always accompanies production of oil. A high viscosity water in oil emulsion, formed in a reservoir or a flowline, causes a significant increase in friction losses resulting in a production decrease. Moreover, natural surfactants, present in oil, may cause suppression of droplet coalescence and, as a result, formation of a stable emulsion that is characterized by a higher viscosity and smaller droplets. In this case, water-oil separation as well as some measurements, regularly conducted in a production tubing, are impaired. Injection of demulsifying chemicals is required to break a stable emulsion. To evaluate consequences of stable emulsion formation and make decision on necessity of demulsifier injection, a reliable model of the emulsification process is needed.

Droplet dispersion can be considered as a sequence of multiple droplet breakup and coalescence events. On large scale, the dispersion process can be most efficiently modelled by a well-known Population Balance (PB) method. There are many droplet breakup and coalescence models available in open literature (Liao and Lucas, 2009, 2010). However, superiority of certain models over others has never been proven.

In the current work, we consider droplet dispersion in a Couette device that consists of two coaxial cylinders (see Fig.1); the inner cylinder rotates whereas the outer is immobile. A flow pattern in such a device is somewhat similar to that in a pipe flow (Eskin et al., 2017); therefore, in some cases low-cost Couette device experiments can successfully substitute costly flow loop tests for laboratory studies of the droplet dispersion process. We will limit our analysis to Couette flows characterized by relatively high Reynolds numbers (Re>13000). In this case, scales of Taylor vorticities become comparable to scales of turbulent fluctuations and the boundary layer theory becomes applicable to a Couette flow (Lewis and Swinney, 1999). The Reynolds number, in this case, is calculated on the basis of the circumferential velocity of the inner cylinder and the Couette device gap.

Eskin et al. (2017) developed a one-dimensional model of droplet dispersion in a Couette device. Modelling was reduced to solution of an Advection-Diffusion-Population Balance equation. The model developed was assumed to be valid for a device, the height of which significantly exceeds the outer radius. The latter condition makes an effect of bottom and upper walls on a flow field to be negligibly small. An applied flow model (Eskin, 2014) was based on the boundary layer theory.

The authors showed that the turbulence energy dissipation rate, which to a great extent determines the rate of droplet breakup and coalescence, is strongly non-uniform across the Couette device gap. The dissipation rate is highest at the inner wall and rapidly reduced to the gap centerline. The processes of droplet breakup and coalescence were modelled by a PB technique. As a breakup kernel, the authors employed the modified model of Coulaloglou and Tavlarides (1977), developed for an inertial regime of turbulence that takes place when sizes of breaking droplets significantly exceed the Kolmogoroff turbulence scale. The improved breakup model assumes the experimentally proven (Kuboi, 1972) three-dimensional Maxwellian distribution of turbulence eddy fluctuation velocity, whereas the original model is based on the unjustified assumption about the 2-D Maxwellian distribution.

The breakup model parameters were identified from the experimental data obtained using a laboratory Couette device. The experimental apparatus was of a relatively small height: the ratio of the outer radius to the gap width was ~1.42. The tests of different durations (2 and 10 min) were conducted for an oil/water mixture, characterized by a small volume fraction of water (2%), in presence of a surfactant suppressing droplet coalescence. The droplet size distributions were determined by analysis of the microscopic images of stabilized emulsion samples using image recognition software ImageJ (NIH). The computations showed that droplets, being dispersed in the laboratory Couette device, reach rather small sizes and are uniformly dispersed over the Couette device radius. The computed cumulative droplet size distributions were relatively close to the measured ones. However, the experimental distributions were wider; i.e., the smallest droplets measured were smaller, whereas the largest were larger than those computed. The authors (Eskin et al., 2017) suggested that this disagreement can be caused by the end effect associated with a small Couette device height, possible droplet coalescence as well partial occurrence of breakup in a viscous regime of turbulence, characterized by droplet sizes to be significantly smaller than the Kolmogoroff scale.

Dispersion of droplets, able to coalesce (no surfactant case), was analysed only numerically. The coalescence kernel of Coulaloglou and Tavlarides (1977) was employed for this purpose. The computations (Eskin et al., 2017) showed that in this case droplets are relatively large and, therefore, strongly stratified across the Couette device gap. An abrupt increase in droplet concentration at the outer wall indicates formation of a water layer. The conclusion was that a Couette device is hardly suitable for studies of turbulent flows of unstable emulsions in a turbulent flow. Therefore, in the present work, we will limit our studies only to modelling the dispersion process in absence of coalescence. We will compare the results, obtained by the engineering model based on the Advection-Diffusion Population Balance equation, with the data produced by the STAR-CCM+ CFD code of Siemens PLM Software in axisymmetric 3D formulation. The adaptive multiple size-groups (A-MuSiG) method,

recently implemented into the code, is employed for population balance modelling. The Reynolds stress turbulence model along with the Daly & Harlow transport model are used for computation of a Couette flow field.

ENGINEERING MODELING APPROACH

Let us formulate and discuss the key modeling assumptions. The critical assumption employed in the current work is that droplets do not coalesce; i.e., an emulsion is stable. Emulsion can be stabilized by an

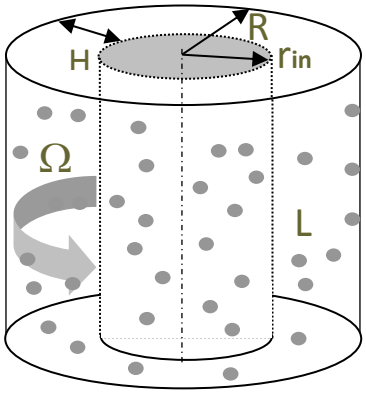

Figure 1: Couette device diagram

addition of chemicals (e.g., asphaltenes or other natural surfactants), molecules of which absorb on droplet surfaces making them rigid and as a result prevent coalescence. For the sake of simplicity, we assume that the emulsion stabilization process is short enough to be neglected. Eskin et al. (2017) showed also that a steady-state droplet size distribution, obtained in a laboratory Couette device in absence of coalescence, was practically independent on an initial droplet size. Also, the dispersion computations conducted for initially monodispersed droplets, uniformly distributed over the Couette device gap, showed that the volume averaged droplet size very rapidly decreases during a short period of stirring. During this initial stirring stage, the droplet size reduction rate greatly decreases and then droplet size distribution slowly approaches the steady-state. Based on these results, we neglect complex effects, associated with initial location of fluids to be stirred, and occurring on the initial dispersion stage. We will also assume that droplets maintain a spherical shape.

Advection – Diffusion – Population Balance approach

Let us formulate the Advection-Diffusion-Population Balance equation for droplets, whose continuous size distribution is substituted with a discrete distribution represented by a finite number of size fractions. Note that in accordance with the analysis of Eskin et al. (2017) we neglect the droplet stratification due to gravity. Then, employment of one-dimensional governing equation is justified and it is written in polar coordinates as follows (Eskin et al., 2017):

$$\frac{\partial N_i}{\partial t} = \frac{1}{r}\frac{\partial}{\partial r} r\left(D_i \frac{\partial N_i}{\partial r} - N_i v_i \right) + \left(\frac{\partial N_i}{\partial t} \right)_{PB}, \quad i=1,\ldots M \qquad (1)$$

where D_i is the turbulent diffusivity of droplets of the i-th size fraction, M is the number of size fractions, N_i is the number concentration of droplets of the i-th size fraction per unit volume, v_i is the radial velocity component of a droplet of the i-th size fraction, and $(\partial N_i/\partial t)_{PB}$ is the concentration change of the i-th size fraction droplets due to both breakup and coalescence (population balance term). All the terms of Eq. (1) are defined by local flow parameters, which can be determined using a simple engineering model of a Couette flow (e.g., Eskin 2010, 2014).

The boundary conditions for this equation are zero droplet fluxes through the inner and outer walls respectively. The corresponding equations for the number droplet fluxes are written as follows:

$$q_i(r_{in}) = \left(D_i \frac{\partial N_i}{\partial r} - N_i v_i \right)\Big|_{r_{in}} = 0 \qquad (2)$$

$$q_i(R) = \left(D_i \frac{\partial N_i}{\partial r} - N_i v_i \right)\Big|_{R} = 0 \qquad (3)$$

where r_{in} and R are radii of the inner and outer Couette device walls respectively.

Distributions of the radial velocity components of droplets and the droplet diffusivities are calculated using the Couette flow model (Eskin et al., 2017). Because droplets are small and the density difference between dispersed and continuous phases is moderate, it is possible to assume that droplets closely follow fluid. Then, the following assumptions are valid: 1) the circumferential velocities of a droplet and a fluid are equal; 2) the turbulent diffusivity of a droplet is equal to the eddy diffusivity. The droplet radial velocity is calculated from the balance between the centrifugal and the radial forces acting on a droplet. To calculate the eddy diffusivity we used the correlation of Notter and Sleicher (1971) for the near-wall region, and the relations, based on the Prandtl mixing length model of turbulence for a core flow (Eskin et al., 2011).

Let us now formulate the population balance term of Eq. (1). Neglecting coalescence we can formulate the corresponding equation for a continuous droplet size distribution as follows:

$$\frac{dN(\upsilon,t)}{dt} = \int_{\upsilon}^{\infty} \beta(\upsilon',\upsilon) G(\upsilon') N(\upsilon',t) d\upsilon' - G(\upsilon) N(\upsilon,t), \qquad (4)$$

where $G(\upsilon')$ is the breakup rate representing the breakup frequency of droplets of volume υ'; $N(\upsilon,t)$ is the number concentration of droplets of volume υ; $\beta(\upsilon',\upsilon)$ is the droplet breakup density function, expressing the number of daughter droplets of size υ formed at breakup of a droplet, whose volume is in the range $\upsilon'+d\upsilon'$.

There are a significant number of different models of droplet breakup (Liao and Lucas, 2009). For all the computations in this work we will employ the modification

(Eskin et al., 2017) of the well-known breakup model of Coulaloglou and Tavlarides (1977). This model is based on the assumption that a droplet can be broken only by an eddy of a scale equal to droplet diameter, whereas distribution of the fluctuation velocity of such an eddy is Maxwellian. The breakup event occurs when the dynamic pressure associated with the eddy fluctuation velocity exceeds the droplet capillary pressure. The Maxwellian distribution assumption is confirmed by the experimental data of Kuboi et al. (1972), who showed that droplet fluctuation velocity distribution in a turbulent flow is nearly Maxwellian and the droplet mean-square velocity is determined as:

$$\left\langle w^2(d)\right\rangle = 2(\varepsilon d)^{2/3} \tag{5}$$

where d is the particle size, ε is the energy dissipation rate per unit mass.

Those experimental results mean that mainly eddies of scales equal to diameters of droplets contribute into dynamics of droplet fluctuations; therefore, such eddies should be major contributors into droplet breakup. Thus, the breakup model of Coulaloglou and Tavlarides (1977) has a reasonably strong physical background.

However, Coulaloglou and Tavlarides (1977) wrongly assumed that the Maxwellian distribution is two-dimensional. Eskin et al. (2017) corrected this flaw by deriving an equation for the breakup rate that accounts for the three-dimensional Maxwellian velocity distribution. Thus, the breakup rate in the present work will be calculated as follows (Eskin et al., 2017):

$$G(\upsilon) = G(d) = K\frac{(\varepsilon d)^{1/3}}{d}\left[erfc(\Phi) + \frac{2}{\pi^{1/2}}\Phi^{1/2}\exp(-\Phi)\right] \tag{6}$$

where $erfc$ is the complementary error function, K is the model parameter, $\Phi = 1.5We_{cr}/We$, $We = 2\rho_f\varepsilon^{2/3}d^{5/3}/\gamma$ is the droplet Weber number, We_{cr} is the critical Weber number, γ is the interfacial tension, ρ_f is the continuous fluid density.

The model parameters K and We_{cr} need to be determined from experimental data.

Let us now formulate assumptions enabling to determine a number and sizes of daughter droplets formed at breakup of a mother droplet. We will employ a regular assumption of binary breakup; i.e., a droplet is always fragmented forming two daughter droplets. There are a number of known breakup density functions β (Liao and Lucas, 2009) determining probability of generation of daughter droplets of a certain volume ratio at a binary breakup event. Most frequently, Π-shaped functions are used for engineering computations. Such functions are characterized by maximum probability of formation of daughter droplets of equal sizes, whereas probability of generation of a droplet of infinitely small size is zero. According to calculations of Eskin et al. (2017), even large variations in shape of a function β do not cause significant changes in a steady-state droplet size distribution computed by the population balance equation. Therefore, following Eskin et al. (2017) in the present work we employed the droplet breakup density function proposed by Lee et al. (1987) that in terms of the breakup volume fraction f_{bv} is formulated as:

$$\beta(f_{bv}) = 12 f_{bv}(1 - f_{bv}), \tag{7}$$

where $f_{bv} = \upsilon/\upsilon'$ characterizes the ratio of the daughter/mother droplet volumes.

In a turbulent flow the droplet breakup rate is mainly determined by the energy dissipation rate. Using the engineering flow model Eskin et al. (2017) calculated the energy dissipation rate as a specific power spent on friction between rotating fluid layers. In a core flow, the energy dissipation rate per unit mass is:

$$\varepsilon = \frac{\tau_{win}u_{o*}}{\rho_f\kappa}\frac{r_{in}^2R}{r^3(r - r_{in})} = \frac{u_{o*}^3}{\kappa}\left(\frac{R}{r}\right)^3\frac{1}{r - r_{in}} \tag{8}$$

at $r_{in} + \delta_{in} \le r \le R_m$,

$$\varepsilon = \frac{\tau_{win}u_{o*}}{\rho_f\kappa}\frac{r_{in}^2R}{r^3(R - r)} = \frac{u_{o*}^3}{\kappa}\left(\frac{R}{r}\right)^3\frac{1}{R - r} \tag{9}$$

at $R_m < r \le R - \delta_o$

where u_{o*} is the friction velocity at the outer cylinder wall, δ_{in} and δ_o are the thicknesses of the viscous layers at the inner and the outer walls respectively, κ is the von-Karman constant, τ_{win} is the shear stress at the outer cylinder wall.

The shear-stress distributions across the viscous layers are nearly constant and, therefore, assumed to be equal to the values calculated on the layer boundaries by Eqs. (8, 9).

The population-balance term in Eq. (1) was computed using the Fixed Pivot method (Kumar and Ramakrishna, 1996). In the computational code developed, the droplet volumes were discretised using a geometrical progression. The smallest droplet size was assumed to be 10% of the lowest value of the Kolmogoroff scale corresponding to the maximum energy dissipation rate that occurs at the inner wall. The radial coordinate along the gap was meshed as follows. The cells adjacent to both the walls were assumed to be equal to the thicknesses of the corresponding viscous layers $\delta_{in} = \delta_o = 11.6\ \delta_w$, where $\delta_w = \mu_f/\rho_f/u_*$ is the wall layer thickness. A geometric progression was used to distribute mesh sizes from the wall to the gap centreline. An explicit finite difference method was employed for numerical solution of Eq. (1). Independence of numerical solution on the chosen discretization of droplet volumes and the gap width, as well on the time step was verified by a number of trial computations.

EXPERIMENT

The breakup model parameters were identified from the laboratory experiments, details of wich are given in Eskin et al. (2017). An available Couette device, regularly used as a laboratory mixer, was employed for this purpose. The inner and the outer cylinder radii of this device are $r_{in} = 14.35$ and $R = 28.7$ mm; i.e., $r_{in}/R = 0.5$. The

relatively small Couette device height, L = 20 mm, leads to a significant effect of the boundary layers at the top and the bottom covers on the flow field (the end effect).

A water-in-oil emulsion, with the water volume fraction

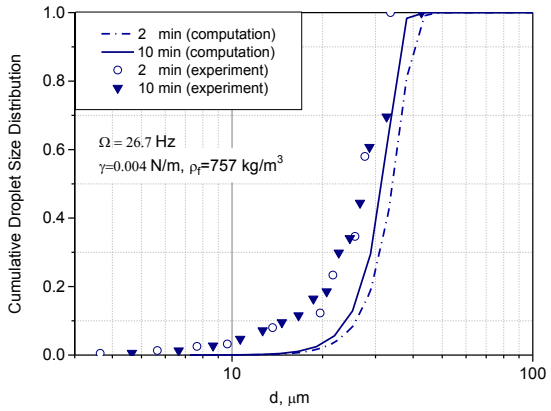

Figure 2: Computed and experimental droplet size distributions for the lower rotation speed

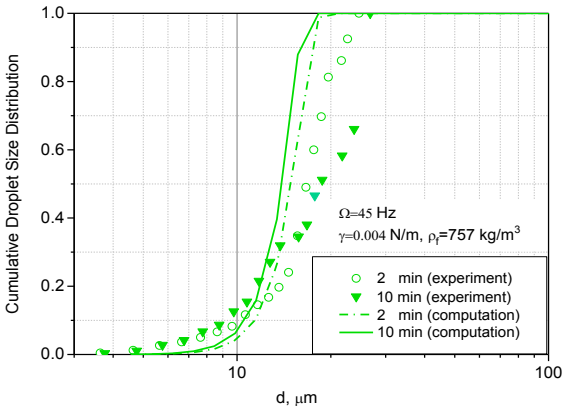

Figure 3: Computed and experimental droplet size distributions for the higher rotation speed

α=0.02 was prepared using mineral oil with the dynamic viscosity μ_f=0.002 Pa s and the density ρ_f=757 kg/m^3 at the temperature 25 °C. Non-ionic surfactant was used for stabilization of dispersed droplets. The surfactant addition led to a significant reduction of the interfacial tension (from γ=0.04 to 0.004 N/m) causing generation of fine droplets. First, the Couette device was filled with the oil, and after that water was added on the top. The experiments were conducted at the defined rotation speeds and mixing durations. After the Couette device was stopped, samples were withdrawn by a pipette from three different locations across the gap. Then, these samples were analysed by a transmitted light microscope and after that the image recognition software was used to determine the droplet size distributions. We would like to emphasize the surfactant caused generation of small droplets, which are uniformly distributed across the gap due to turbulent dispersion; therefore, the droplet size distributions measured at the different locations were almost identical.

Based on the experimental data obtained for the two different rotation speeds, Ω=26.6 and 45 Hz, and the two different stirring durations, 2 and 10 min, we identified the breakup model parameters in Eq. (6) as follows: $K = 1$ and $We_{cr} = 0.5$. The identification accuracy was to some extent impaired due to the limited experimental data for different durations, the end effect, partial shift of the breakup regime from the inertial subrange of turbulence to the viscous subrange, and not entirely suppressed droplet coalescence.

COMPUTATIONAL FLUID DYNAMICS – POPULATION BALANCE MODELLING

The A-MuSiG method employed is adaptive; i.e., size discretization of a dispersed phase varies during computations as a result of breakup and coalescence. For each size fraction (size-group), its own mass and (if necessary) momentum balance equations can be formulated. The instantaneous mass balance equation for the i-th size fraction in a turbulent flow is:

$$\frac{\partial \alpha_i \rho_d}{\partial t} + \nabla \cdot \left(\alpha_i \rho_d \boldsymbol{u_i}\right) = \sum_j \left(\dot{m}_{ij} - \dot{m}_{ji}\right) \quad (10)$$

where $\dot{m}_{ij}$ is the mass transfer rate from the j-th to the i-th size fraction, $\boldsymbol{u_i}$ is the average velocity of the i-th size fraction, α_i is the Reynolds averaged (RA) volume concentration of the size fraction i, ρ_d is the droplet density.

The fraction-to-fraction mass transfer occurs due to breakup and coalescence, e.g., if a droplet is broken by turbulence, its mass and momentum are redistributed among smaller size fractions.

The RA Navier-Stokes (RANS) equations for the i-th size fraction of the dispersed phase are:

$$\frac{\partial \alpha_i \rho_d \boldsymbol{u_i}}{\partial t} + \nabla \cdot \left(\alpha_i \rho_d \boldsymbol{u_i u_i}\right) = -\nabla P - \nabla \cdot \boldsymbol{\tau_R} + \sum_j \left(\dot{m}_{ij} \boldsymbol{u_j} - \dot{m}_{ji} \boldsymbol{u_i}\right), \quad (11)$$

where $\boldsymbol{\tau_R}$ is the Reynolds stress.

It was assumed that the flow field is axisymmetric. Our experience shows that not every RANS model is capable to reproduce the swirl flow field: both $k-\varepsilon$ and $k-\omega$ models underestimate the torque at the Couette device spindle approximately by a factor of two. In the present study, we use the Reynolds-stress, linear pressure-strain turbulence model with the Daly-Harlow tensor diffusivity. The model predictions are in a very good agreement with the experimental data (Lewis and Swinney, 1999).

In the A-MuSiG method the number density equation is solved for each size fraction:

$$\frac{\partial N_i}{\partial t} + \nabla \cdot \left\{ N_i \left(\boldsymbol{u_i} + D_i \nabla \ln \upsilon_i \right) \right\} = S_i, \quad (12)$$

where S_i is source term due to breakup and coalescence. As one can see, the volume of a single droplet $\upsilon_i = \alpha_i / N_i$ is not prescribed a priory but varies in both time and space; it makes the method adaptive and our experience shows that from 3 to 7 size-fractions are sufficient for reliable engineering estimates.

One can see that there is an extra transport (diffusive) term in Eq. (12) that appears as a result of Reynolds-averaging of the instantaneous equation for N_i. The derivation details are given in Vikhansky and Splawski (2015).

As one can see, Eqs. (10)-(12) are presented in the standard form of multiphase fluid dynamics. A population balance

algorithm enters into these equations only through their source terms S_i, $\dot{m}_{ij}$. In the present study, the source terms are calculated by the direct quadrature spanning tree method (Vikhansky, 2013).

Computational examples

Examples are given for the laboratory Couette device employed in the present work for dispersion of water in mineral oil in presence of an emulsifying surfactant. The volume water fraction was fixed, α=0.02. Other details of the experiments are given in the section "Experiment'.

Let us start with a brief illustration of one-dimensional model performance that was in detail analysed by Eskin et al. (2017).

In Figs. 2, 3 we showed the experimental and computed cumulative droplet size distributions obtained in the Couette device at the spindle rotation speeds Ω=26.7 and 45 Hz respectively. The data are presented for the 2 and 10 min operation durations. Only droplet breakup was taken into account in the computations.

One can see that an increase in the spindle rotation speed leads to a significant droplet size reduction. Also, it is worth to note that the size distributions obtained during 2 and 10 min of operation are close to each other. Thus, the most intense dispersion occurs during a relatively short initial time period. The computed size distributions are noticeably narrower than the experimental ones. This disagreement is mainly caused by neglecting a coalescence, not fully supressed by the surfactant, a limited accuracy of the 1-D model and the end effect associated with the relatively small Couette device height (see the brief discussion in "Introduction).

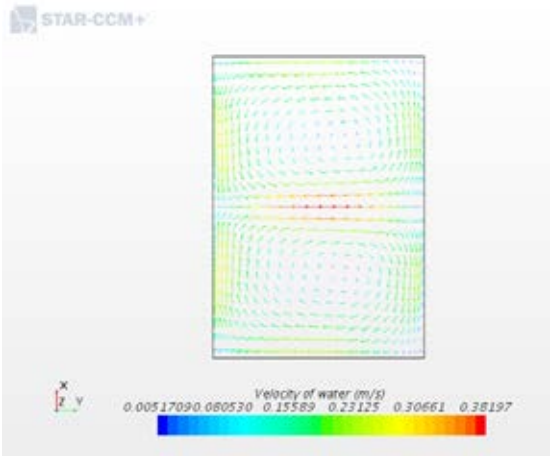

Figure 4: Distribution of the axial (x) and radial (y) velocity components over the radial Couette device gap cross-section.

Computations of droplet dispersion by the CFD code allowed us to better understand underlying process physics. The circumferential flow velocities in the investigated Couette flow regimes reach several meters per second. However, because the Couette device employed has relatively small height, secondary flows caused mainly by the end effect can be of relatively high intensities. The calculated velocity field of the secondary flows at the rotation speed Ω=26.7 Hz is shown in Fig.4. One can see the two nearly symmetric recirculation cells, characterized by velocities, which are relatively small but significant enough to strongly influence droplet transport across the Couette device gap. Thus, accounting for the secondary flows is one of important advantages of the 3-D simulations over the 1-D model calculations.

Also, the end effect significantly reduces accuracy of computations of the shear stresses at the inner and the outer cylinders of the Couette device by the 1-D model. Stress distributions at both the cylinders are shown in Fig.5. The distributions are strongly non-uniform. Moreover, the mean stress at the inner cylinder wall is equal to 21.9 Pa, whereas at the outer cylinder - 3.38 Pa. For the given radii ratio of the cylinders, the 1-D model predicts the shear stress at the outer cylinder wall to be 5.48 Pa that by factor 1.6 exceeds the stress calculated by the 3-D code. This difference is caused by the end effect that is expected to decrease with an increase in the Couette device height.

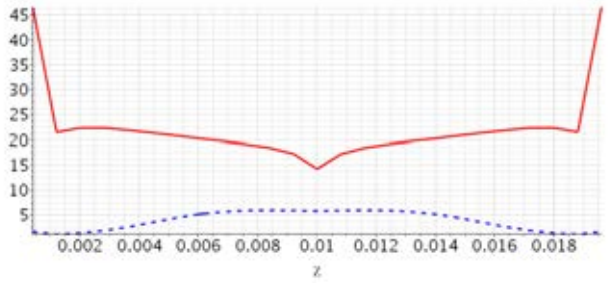

Figure 5: Shear stress (Pa) at the internal (solid line) and the external (dashed line) cylinder walls.

Let us now discuss the droplet dispersion results. The 3-D code, employing the same breakup kernel, Eq. (6), provides droplet size distributions, which are similar to those obtained using the 1-D model (Figs. 2, 3). I.e., the computed size distributions are still significantly narrower than the experimental ones. A highly possible reason of this discrepancy is that droplet coalescence was not entirely supressed (Eskin et al., 2017) by surfactant. The discussion of this phenomenon is given in Eskin et al. (2017). Therefore, in further calculations by the 3-D code, besides breakup, we will also artificially introduce coalescence to more accurately fit the experimental data.

For coalescence modelling, we formally employ the model of Coulaloglou and Tavlarides (1977). Whereas the droplet collision rate, used in the present work, is exactly equal to that in Coulaloglou and Tavlarides (1977), the equation for the coalescence efficiency of the droplets of sizes d_i and d_i is different from the original one and written as:

$$\lambda_{ij} = \exp\left(- C \frac{\rho_f \mu_f \varepsilon d_{ij}^2}{\gamma^2} \right), \qquad (13)$$

where $d_{ij} = d_i d_j / \left(d_i + d_j \right)$, C is the empirical coefficient, μ_f is the continuous fluid dynamic viscosity. Note, in Coulaloglou and Tavlarides (1977) one can find d_{ij}^4 (not d_{ij}^2) under the exponent. The authors of the model made a trivial typo in the derivations. Unfortunately, the erroneous equation has been widely used by numerous authors (e.g., Liao and Lucas, 2010).

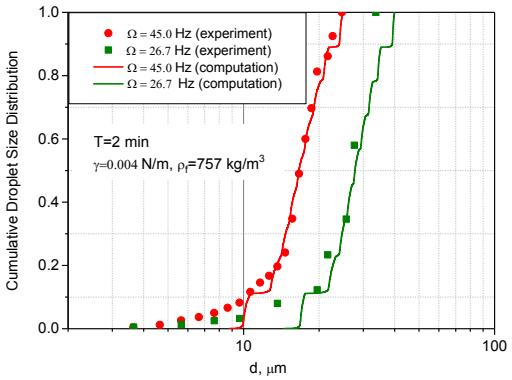

Figure 6: Cumulative size distribution for the 26.6 (right) and 45 Hz (left) rotation speeds: the experimental data (markers) and the CFD code (solid lines).

In the 3-D computations we use the same value of We_{cr} as in the 1-D case ($We_{cr} = 0.5$). The coalescence related empirical coefficient, identified from the experimental droplet size distributions, is $C = 3 \cdot 10^6$. The calculated droplet size distributions for the 2-min duration experiments are shown in Fig.6. One can see a rather good agreement between the computed and the experimental curves. Note that the computations do not predict the left size distribution tales, caused by presence of small particles, because of the relatively small number of size fractions (9) employed for the 3-D computations.

We would like to also emphasize that Eq. (13) was derived assuming mobile droplet interfaces. In this work, we use this equation for modelling coalescence in presence of a surfactant that greatly reduces interface mobility. Thus, employment of Eq. (13) here does not have a solid physical justification and serves only for fitting the experimental data; therefore, the empirical coefficient identified is not suitable for modelling dispersion of fluids different from those used in the present work.

To illustrate the dispersion process mechanisms, in Fig.7 we plotted the distributions of both the breakup and coalescence rates over the Couette device gap under steady -state conditions at the rotation speed Ω=26.7 Hz. Note that the breakup plot is shown using logarithmic scale, whereas the coalescence plot - linear scale. As one can see, the breakup zone is located in the vicinity of the inner wall, where the turbulent dissipation rate is highest. In contrast to breakup, the coalescence rate is highest in the centres of the recirculation zones. We would like to also emphasize that the maximum breakup rate is much higher than the maximum coalescence rate. However, the total coalescence zone is much larger than the breakup one; therefore the total number of coalescence events is matched by the total number of breakup events.

To evaluate mixing quality in the considered Couette device, in Fig.8 we showed the steady-state distribution of the droplet Sauter diameter over the gap. Relatively small variations of this parameter over the gap, except the inner wall vicinity, show that the dispersed system is well-mixed. This observation means that the turbulent diffusion of droplets significantly contributes into droplet dispersion.

Thus, we performed a detailed studies of dispersion of chemically stabilized water droplets in a turbulent Couette flow using both the engineering 1-D model and the 3-D CFD code. Formal accounting for coalescence in 3-D modelling allowed to accurately fit the experimental data.

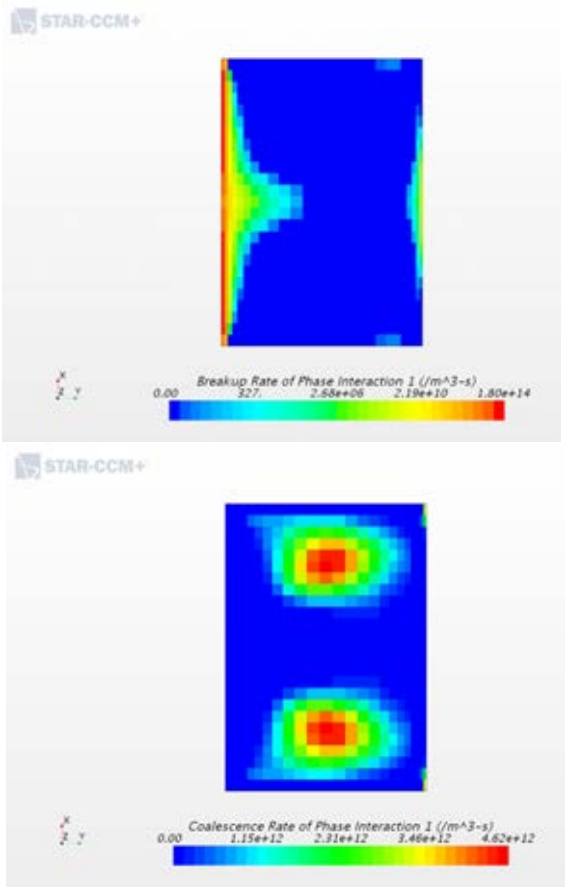

Figure 7: Distributions of the steady-state breakup (upper) and the coalescence (bottom) rates over the Couette device gap, Ω=26.7 Hz.

A number of the 3-D computations allowed us to reveal some peculiarities of the dispersion process. However, employment of the artificial approach to accounting for coalescence of partially stabilized droplets limits application of the identified model parameters to only the dispersion system that was studied in the current work.

CONCLUSIONS

Dispersion of chemically stabilized water droplets in a turbulent Couette flow has been studied by both the 1-D and 3-D models. The 1-D model is based on solution of the Advection-Diffusion Population Balance equation. Three-dimensional modelling has been conducted using the CFD-population balance A-MuSiG method recently implemented into the STAR-CCM+ code of Siemens PLM Software. The same droplet breakup model has been employed for both the models. The 3-D computations revealed relatively intense circulation motion caused by the Couette device cover walls. Nevertheless, the droplet size distributions predicted by both the models were close to each other. An analysis of the experimental data showed that droplet coalescence is not fully supressed by the surfactant; therefore, a coalescence was formally

introduced into the 3-D dispersion model to accurately fit the experimental data. The 3-D computations showed also that the dispersed phase is rather uniformly distributed over the Couette device gap that indicates a significant contribution of turbulent diffusion into the dispersion process.

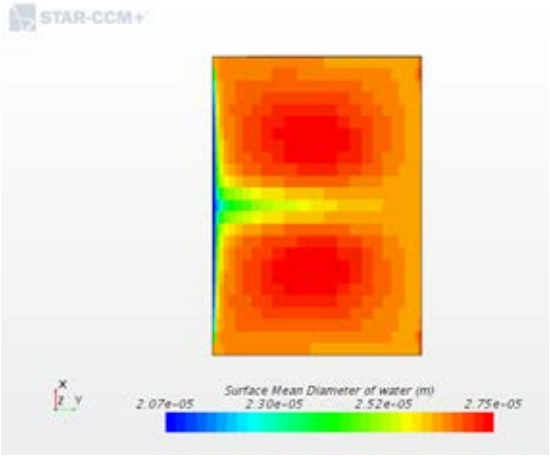

Figure 8: Distribution of the droplet Sauter diameter over the Couette device gap, Ω=26.7 Hz.

REFERENCES

COULALOGLOU C.A., TAVLARIDES L.L., (1977), "Description of interaction processes in agitated liquid-liquid dispersions", *Chem. Eng. Sci*., **32**, 1289-1297.

ESKIN D., RATULOWSKI J., AKBARZADEH K., PAN S., (2011), "Modelling asphaltene deposition in turbulent pipeline flows", *The Can. J. Chem. Eng.,* **89**, 421-441.

ESKIN D., (2014), "Applicability of a Taylor-Couette device to characterization of turbulent drag reduction in a pipeline", *Chem. Eng. Sci.,* **116**, 275-283.

ESKIN D., TAYLOR S., YANG D., (2017), "Modeling of droplet dispersion in a turbulent Taylor–Couette flow", *Chem. Eng. Sci.,* **161**, 36–47.

KUBOI R., KOMASAWA I., and OTAKE T., (1972), "Behavior of dispersed particles in turbulent liquid flow", *J. Chem. Eng. Japan*, **5**, 349-355.

KUMAR S., RAMAKRISNA, D., 1996. On the solution of population balance equations by discretization-I. A fixed pivot technique. Chem. Eng. Sci. 51, 1311-1332.

LEE C.H., GLASGOW L.A., ERICKSON L.E., (1987), "Bubble breakup and coalescence in turbulent gas-liquid dispersions", *Chem. Eng. Commun*., **59**, 65-84.

LEWIS G.S., SWINNEY H.L., 1999, "Velocity structure functions scaling and transitions in high-Reynolds-number Couette–Taylor flow", *Phys. Rev. E*, **59**, 5457-5467.

LIAO Y., LUCAS D., (2009), "A literature review of theoretical models for drop and bubble breakup in turbulent dispersions", *Chem. Eng. Sci*., **64**, 3389-3406.

LIAO Y., LUCAS D., (2010), "A literature review on mechanisms and models for the coalescence process of fluid particles", *Chem. Eng. Sci.,* **65**, 2851-2864.

NOTTER R.H., SLEICHER C.A., (1971), "The eddy diffusivity in the turbulent boundary layer near a wall", *Chem. Eng. Sci.,* **26**, 161-171.

VIKHANSKY A., (2013), "Direct quadrature spanning tree method for solution of the population balance equations", *Journal of Aerosol Science*, **55**, 78-88.

VIKHANSKY A., SPLAWSKI A., (2015), "Adaptive multiple size group method for CFD-population balance modelling of polydisperse flows", *The Can. J. Chem. Eng.*, **93**, 1327-1334.